J Physiol 593.18 (2015) pp 4181–4199

The Journal of Physiology

ClC-1 mutations in myotonia congenita patients: insights into molecular gating mechanisms and genotype–phenotype correlation

P. Imbrici[1], L. Maggi[2], G. F. Mangiatordi[1], M. M. Dinardo[1], C. Altamura[1], R. Brugnoni[2], D. Alberga[3], G. Lauria Pinter[4], G. Ricci[5], G. Siciliano[5], R. Micheli[6], G. Annicchiarico[7], G. Lattanzi[3], O. Nicolotti[1], L. Morandi[2], P. Bernasconi[2], J.-F. Desaphy[1], R. Mantegazza[2] and D. Conte Camerino[1]

[1] *Department of Pharmacy – Drug Sciences, University of Bari, Bari, Italy*
[2] *Neuroimmunology and Neuromuscular Diseases Unit, IRCCS Fondazione Istituto Neurologico 'Carlo Besta', Milano, Italy*
[3] *Department of Physics 'M. Merlin', INFN and TIRES, University of Bari, Bari, Italy*
[4] *Neuroalgology and Headache Unit, IRCCS Fondazione Istituto Neurologico 'Carlo Besta', Milano, Italy*
[5] *Department of Clinical and Experimental Medicine, Section of Neurology, University of Pisa, Pisa, Italy*
[6] *Unit of Child Neurology and Psychiatry, Spedali Civili, Brescia, Italy*
[7] *Regional Coordination for Rare Diseases, A. Re. S. Puglia, Bari, Italy*

Key points

- Loss-of-function mutations of the skeletal muscle ClC-1 channel cause myotonia congenita with variable phenotypes.
- Using patch clamp we show that F484L, located in the conducting pore, probably induces mild dominant myotonia by right-shifting the slow gating of ClC-1 channel, without exerting a dominant-negative effect on the wild-type (WT) subunit.
- Molecular dynamics simulations suggest that F484L affects the slow gate by increasing the frequency and the stability of H-bond formation between E232 in helix F and Y578 in helix R.
- Three other myotonic ClC-1 mutations are shown to produce distinct effects on channel function: L198P shifts the slow gate to positive potentials, V640G reduces channel activity, while L628P displays a WT-like behaviour (electrophysiology data only).
- Our results provide novel insight into the molecular mechanisms underlying normal and altered ClC-1 function.

Abstract Myotonia congenita is an inherited disease caused by loss-of-function mutations of the skeletal muscle ClC-1 chloride channel, characterized by impaired muscle relaxation after contraction and stiffness. In the present study, we provided an in-depth characterization of F484L, a mutation previously identified in dominant myotonia, in order to define the genotype–phenotype correlation, and to elucidate the contribution of this pore residue to the mechanisms of ClC-1 gating. Patch-clamp recordings showed that F484L reduced chloride currents at every tested potential and dramatically right-shifted the voltage dependence of slow gating, thus contributing to the mild clinical phenotype of affected heterozygote carriers. Unlike dominant mutations located at the dimer interface, no dominant-negative effect was observed when F484L mutant subunits were co-expressed with wild type. Molecular dynamics simulations further revealed that F484L affected the slow gate by increasing the frequency and stability of the H-bond formation between the pore residue E232 and the R helix residue Y578. In addition, using patch-clamp electrophysiology, we characterized three other myotonic ClC-1 mutations.

D. Conte Camerino and R. Mantegazza contributed equally to this work.

DOI: 10.1113/JP270358

We proved that the dominant L198P mutation in the channel pore also right-shifted the voltage dependence of slow gating, recapitulating mild myotonia. The recessive V640G mutant drastically reduced channel function, which probably accounts for myotonia. In contrast, the recessive L628P mutant produced currents very similar to wild type, suggesting that the occurrence of the compound truncating mutation (Q812X) or other muscle-specific mechanisms accounted for the severe symptoms observed in this family. Our results provide novel insight into the molecular mechanisms underlying normal and altered ClC-1 function.

(Received 13 February 2015; accepted after revision 4 June 2015; first published online 12 June 2015)
Corresponding author P. Imbrici, Department of Pharmacy – Drug Sciences, University of Bari, Via Orabona 4, 70125 Bari, Italy. Email: paola.imbrici@uniba.it

Abbreviations CBS, cystathionine-β-synthase; H-bond, hydrogen bond; MC, myotonia congenita; MD, molecular dynamics; WT, wild type.

Introduction

Myotonia congenita (MC) is the most common skeletal muscle inherited channelopathy (Horga *et al.* 2013). It is clinically characterized by muscle stiffness after a voluntary movement that is worse after rest and improves with repeated activity (the so-called 'warm up' phenomenon). Inheritance mode is dominant (Thomsen disease) or recessive (Becker disease), with a more severe phenotype in the latter form (Colding-Jorgensen, 2005; Lossin & George, 2008; Raja Rayan & Hanna, 2010; Burge & Hanna, 2012; Lo Monaco *et al.* 2014). Loss-of-function mutations in the *CLCN1* gene encoding the skeletal muscle voltage-gated ClC-1 chloride channel are the primary contributors to the pathogenesis of MC (Koch *et al.* 1992; George *et al.* 1993). The ClC-1 channel, which is located at the T-tubules and sarcolemma in skeletal muscle, normally works to dampen abnormal membrane excitability and stabilize the resting membrane potential after an action potential (Lossin & George, 2008). Thus, the reduced chloride conductance resulting from MC mutations will predispose the sarcolemma to spontaneous action potential runs or abnormal afterdischarges that hamper muscle relaxation after contraction, causing myotonia (Lossin & George, 2008; Burge & Hanna, 2012).

So far more than 130 mutations have been identified over the entire length of the channel (Lossin & George, 2008; Matthews *et al.* 2010; Raja Rayan & Hanna, 2010; Burge & Hanna, 2012; Brugnoni *et al.* 2013). The functional analysis of naturally occurring ClC-1 mutations in heterologous expression systems, as well as in animal models, has provided important insights into the structure and function of the channel and into the pathomechanism of the disease (Pusch *et al.* 2002; Desaphy *et al.* 2013; Ha *et al.* 2014). However, various aspects of channel gating, disease pathogenesis, clinical manifestation, and their close connections, remain to be clarified. Indeed, although it is necessary to understand the correlation between clinical symptoms, genetic defects and mode of MC inheritance, in order to match patients with specific therapies, this is not easily predictable, given the variety of symptoms reported among individuals carrying the same ClC-1 mutation (Colding-Jorgensen *et al.* 2005). Notably, direct activators of ClC-1 channels have not yet been identified, thereby precluding a personalized therapy for MC patients. Currently, the sodium channel blocker mexiletine represents the first line therapy, but its use is limited by poor tolerability, and a suboptimal or negative response in a proportion of patients. In addition, two carbonic anhydrase inhibitors, acetazolamide and dichlorphenamide, have been used empirically in MC with variable results (Griggs *et al.* 1978; Matthews *et al.* 2010; Markhorst *et al.* 2014; Trivedi *et al.* 2014). Importantly, it would be very useful to define the ClC-1 structural determinants involved in channel gating in order to understand the pathomechanisms of MC and to address drug targeting.

The functional ClC-1 channel is a homodimer with a double-barrelled architecture, in which fast gating controls the opening and closing of individual protopores, whereas slow gating results from cooperative interactions between the two pores (Saviane *et al.* 1999; Accardi & Pusch, 2000; Dutzler, 2006). Remarkably, defects in the fast and slow gating modes of the channel have been proposed to explain the molecular mechanisms of dominant and recessive inheritance of MC (Accardi & Pusch, 2000; Simpson *et al.* 2004; Weinberger *et al.* 2012; Ha *et al.* 2014). As a general rule, recessive ClC-1 mutations are expected to affect the fast gate of individual subunits, causing different degrees of haploinsufficiency (Matthews *et al.* 2010; Raja Rayan & Hanna, 2010). On the other hand, dominant mutations are expected to exert a dominant-negative effect on the associated wild-type subunit by disrupting the slow gate of the channel, thereby altering or impairing the dimerization process (Matthews *et al.* 2010). As the slow gate was originally supposed to involve interaction between subunits through helices at the dimer interface (Duffield *et al.* 2003), this mechanistic hypothesis easily fitted with dominant mutations that were detected preferentially on the boundary region between two

monomers, indicated as a hot spot (Pusch *et al.* 1995; Fialho *et al.* 2007; Skalova *et al.* 2013).

Interestingly, the molecular determinants of the slow gate are still awaiting elucidation. Far from involving merely helices and residues at the dimer interface (Duffield *et al.* 2003), an emerging view of the mechanism of cooperative gating predicts concerted interactions between the residue E232 in the channel pore, the boundary region (comprising helices H, I, G), and the C-terminal CBS domains via helix R (Duffield *et al.* 2003; Estevez *et al.* 2004; Cederholm *et al.* 2010; Feng *et al.* 2010; Ma *et al.* 2011; Bennetts & Parker, 2013). A recent report proposed that slow channel closure may depend on the H-bond interaction established by E232 of pore helix F and Y578 of helix R (Bennetts & Parker, 2013). The further observation that ClC-1–ClC-2 heterodimeric channels lack cooperative gating (Stölting *et al.* 2014*b*) suggests that slow gating of ClC channels arises from conformational changes within the individual protopore.

These more recent mechanistic hypotheses on gating modes substantially challenge the general held view about the pathomechanism, mode of inheritance, and preferential location for dominant and recessive MC mutations. Therefore, it remains to be ascertained whether MC mutations outside the dimer interface might be inherited in a dominant manner (or cause dominant myotonia), and lead to the simultaneous disturbance of the two pores.

In this study we provide an in-depth characterization of the F484L ClC-1 mutation through medical diagnosis, patch-clamp electrophysiology and molecular dynamics. This mutation lies outside the dimer interface, in helix N, which is involved in the ion conductive pathway (Dutzler *et al.* 2002, 2003; Skalova *et al.* 2013), and is dominantly inherited (Brugnoni *et al.* 2013). It is also in close proximity to the E232 and Y578 residues involved in slow gating (Bennetts & Parker, 2013). In addition, we present the clinical and electrophysiological analysis of three other ClC-1 mutants associated with MC: the dominant L198P mutation located in the pore, and the recessive L628P and V640G mutations located in the CBS1 domain (Brugnoni *et al.* 2013; Lakraj *et al.* 2013). These ClC-1 mutations have been previously identified in MC patients, but have never been characterized before (Brugnoni *et al.* 2013; Lakraj *et al.* 2013). It is expected that such characterization would contribute to clarify the genotype–phenotype correlation and to gain insights into the mechanisms underlying ClC-1 function.

Methods

Genetic diagnosis

Genomic DNA was extracted from peripheral blood, collected in EDTA-containing tubes, by standard procedures and screened for CLCN1 mutations by PCR analysis of the 23 exons, as previously described (Brugnoni *et al.* 1999, 2013). Written informed consent for DNA storage and use for genetic analysis and research purposes was obtained from all patients (parents or tutors for patients under age) and relatives, as required by the Ethical Committee of the Fondazione Istituto Neurologico 'Carlo Besta' in accordance with the *Declaration of Helsinki*.

Clinical diagnosis

We investigated four families with clinically and genetically defined MC, including five patients presenting at ages ranging between 1 and 20 years. All patients were referred to our clinics due to variable grades of muscle stiffness. Neurological examination was specifically conducted searching for myotonic signs such as tongue, eyelid, lid-lag, jaw myotonia, handgrip and percussion myotonia.

Mutagenesis and expression of hClC-1 WT and mutant channels

Mutations were introduced into the plasmid pRcCMV-hClC-1 containing the full-length wild-type (WT) hClC-1 cDNA using the QuikChange site-directed mutagenesis kit (Agilent Technologies, Santa Clara, CA, USA), as previously described (Desaphy *et al.* 2013). The complete coding region of the cDNA was sequenced to exclude polymerase errors. The tsA cells were transiently transfected with a mixture of the hClC-1 (5 μg) and CD8 reporter plasmids (1 μg) using the calcium–phosphate precipitation method. Cells were examined between 36 and 80 h after transfection. Only cells decorated with anti-CD8 antibody-coated microbeads (Dynabeads M450, Invitrogen) were used for patch-clamp recordings.

Electrophysiology and data analysis

Standard whole-cell patch-clamp recordings were performed at room temperature (~20°C) using an Axopatch 200B amplifier (Axon Instruments). The composition of the extracellular solution was (in mM): 140 NaCl, 4 KCl, 2 $CaCl_2$, 1 $MgCl_2$ and 5 Hepes, and the pH was adjusted to 7.4 with NaOH. The high-chloride pipette solution contained (in mM): 130 CsCl, 2 $MgCl_2$, 5 EGTA and 10 Hepes, and the pH was adjusted to 7.4 with CsOH. In this condition, the equilibrium potential for chloride ions was about −2.8 mV and cells were clamped at the holding potential (HP) of 0 mV. In the low-chloride internal solution, caesium chloride was replaced by caesium glutamate. With this pipette solution, the equilibrium potential for chloride ions was about –92 mV and cells were clamped at the HP of –95 mV. Pipettes were pulled from borosilicate glass and had ~3 MΩ resistance, when filled

with the above pipette solutions. Currents were low-pass filtered at 2 kHz and digitized with sampling rates of 50 kHz using the Digidata 1440A AD/DA converter (Axon Instruments). Patches with a series resistance voltage error greater than 5 mV and those with non-negligible leak current were discarded. Chloride currents were recorded ∼5 min after achieving the whole-cell configuration, to allow the pipette solution to equilibrate with the intracellular solution.

Voltage-dependent channel activity was measured by applying specific voltage step pulses from the HP depending on the internal chloride concentration, as described in the Results section and shown in the figures. We measured the *I–V* relationship and the overall apparent open probability in high-chloride (134 mM) intracellular solutions to enhance current amplitude and in more physiological low internal chloride (4 mM) solutions. In high-chloride solution voltage steps were applied from −200 mV to +200 mV in 10 mV intervals, each followed by a voltage step at −105 mV where tail currents were measured. In low-chloride solution, currents were elicited by voltage steps between −180 mV and +180 mV in 10 mV intervals, followed by a test pulse to −105 mV. Voltage steps were applied every 3 s to allow complete recovery of current amplitude at the HP between two pulses. The instantaneous and steady-state current–voltage relationships were drawn by measuring instantaneous and steady-state current densities (pA pF^{-1}) at the beginning (∼1 ms) and end (∼390 ms) of each voltage step. Overall apparent open probability (P_o) for WT and mutant channels was obtained from normalized peak tail currents (Desaphy *et al.* 2013) using test steps to −105 mV for 100 ms after 400 ms conditioning pulses in the range from −200 mV to +200 mV from a holding potential of 0 mV (or −95 mV). Voltage dependence of channel activation was determined by plotting the apparent open probability (P_o) as a function of the voltage of the preceding pulses. The points were fitted with a Boltzmann function:

$$P_o(V) = P_{min} + (1 - P_{min})/\{1 + \exp[(V - V_{0.5})/k]\},$$

where P_{min} is the minimal value of P_o, $V_{0.5}$ is the half-maximal activation potential, and k is the slope factor. Unless otherwise specified, these sequences were repeated every 3 s, this lapse between two depolarizing steps being long enough to maintain a constant current at the holding level. Open probability for slow gating ($P_{o,slow}$) was obtained by using a similar protocol to that for the overall P_o (200 ms conditioning pulse), except that an extra 400 μs activation pulse to +180 mV was added before stepping to −105 mV. This very positive step fully activates (opens up) the fast gates of the channel and the tail currents at −105 mV then reflect only slow gating (Accardi & Pusch, 2000). Since overall apparent open probability equals the product of its fast and slow components, open probability of the fast gates ($P_{o,fast}$) could then be calculated for a given test voltage by dividing the relevant P_o by its corresponding $P_{o,slow}$ (Accardi & Pusch, 2000; Duffield *et al.* 2003). Apparent P_o, $P_{o,slow}$ and $P_{o,fast}$ were calculated from normalized instantaneous current amplitude measured at the beginning of the tail pulse at −105 mV. The voltage dependence of channel activation was examined by plotting the apparent open probability (P_o) as a function of membrane potential at the end of the test pulse. The relationship was fitted with a Boltzmann function. Data were analysed off-line by using pClamp 10.3 (Axon Instruments) and Kaleida Graph Software. Results are reported as means ± SEM from n cells, and statistical analysis was performed using Student's t test, with $P < 0.05$ or less considered as significant.

Molecular dynamics

The homology model of ClC-1, recently published by Bennetts & Parker (2013), was used as starting system. It consists of the ClC-1 dimer based on the crystallographic coordinates of CmClC (PDB id: 3ORG; Feng *et al.* 2010). For the sake of computational time, the C-terminal (from residue 588) was excluded from the model. The resulting structure was first pre-treated using the protein preparation wizard (Version 9.5) (Schrödinger Release 2013-2), which enables addition of missing hydrogen atoms and determination of the optimal tautomer for histidine residues. The simulation system was built as follows: A 110 × 140 $Å^2$ POPC (1-palmitoyl,2-oleoyl-*sn*-glycero-3 phosphocholine) bilayer patch was first built using the membrane plugin of VMD (Visual Molecular Dynamics) (Humphrey *et al.* 1996), with the membrane aligned with the z-axis. The ClC-1 dimer was embedded in this bilayer and lipid molecules within 0.6 Å of heavy atoms of the protein were removed. To neutralize the system, 47 Na^+ and 65 Cl^- ions were added using VMD's autoionize plugin, generating a 150 mM ionic concentration and a final system of 136784 atoms (number computed for wild type). Both F484L and WT protein structures were incorporated into a periodic box of TIP3P water molecules (Jorgensen *et al.* 1983) extended by 18 Å in each direction from all protein atoms using the Add Solvation Box plugin of VMD. All MD simulations were performed using NAMD 2.9 (Phillips *et al.* 2005) and the CHARMM27 force field (MacKerell *et al.* 2000). The 'useConstantArea' option was set 'on' in order to keep realistic lipid structures. The full system was minimized to remove steric clashes in the initial geometry and gradually heated up to 310 K within 500 ps of MD. The SHAKE algorithm was employed to constrain all R–H bonds (Miyamoto & Kollman, 1992). Rigid water molecules were implemented using the SETTLE algorithm (Ryckaert

et al. 1977). Periodic boundary conditions were applied in all directions. A non-bonded cut-off of 12 Å was used, whereas the Particle-Mesh-Ewald (PME) (Darden *et al.* 1993) was employed to include the contributions of long-range interactions. All simulations were performed in an isothermal–isobaric ensemble (1 atm, 310 K) using a modified Nosé–Hoover method, in which Langevin dynamics is used to control fluctuations in the barostat, as implemented in NAMD 2.9 (Martyna *et al.* 1994) (oscillation period 200 fs, decay coefficient 100 fs), and a Langevin thermostat (Adelman & Doll, 2008) (damping coefficient 1 ps^{-1}). The time step was set to 2 fs, and coordinates were saved every 5000 steps (10 ps). A MD trajectory of 25 ns was obtained for the wild type and the mutated form. For each system investigated, the equilibration of the structure required less than 5 ns and thus the first 5 ns were removed from the analysis.

Molecular visualization system

To visualize the ClC-1 3D structure and the position of mutated residue, the homology model was rendered using Pymol (http://www.pymol.org/).

Results

The four mutations studied here were previously identified in a large cohort of myotonia congenita probands (Brugnoni *et al.* 2013).

Clinical phenotype of four Italian MC families

Family 1. A single c.1450T>C transition (F484L) was observed in two members of the same family. The proband is now 75-year-old man and presented at the age of 18 years with lower limb muscle stiffness, developing mainly at the beginning of movement after prolonged rest and improving with exercise. His son, now 50 years old, noticed the same symptoms at the age of 20. Neither of them reported cold-aggravated or painful myotonia. Neurological examination revealed myotonia with warm-up phenomenon mainly in quadriceps and hands, in association with diffuse muscle hypertrophy; no muscle weakness was observed. Symptoms remained stable over the years and both patients practiced sport activities without any limitation. Clinical features and inheritance were in agreement with Thomsen disease. The son was administered mexiletine with mild benefit, while the father has never taken any treatment for myotonia. Both patients underwent electromyography with a short exercise test with and without cooling, as reported by Fournier and colleagues (Fournier *et al.* 2006), revealing a pattern II typical of myotonia congenita. In addition the father's neurophysiological examination showed a worsening after cooling, which was suggestive of dominant MC.

Family 2. A single c.593T>C transition (L198P) was detected in a male, now 24 years old, who presented at the age of 8 with stiffness when initiating a movement after prolonged rest, initiating in the lower limb and then extending to hands and facial muscles, including masseter. The clinical course was stable over the years and myotonia remained predominant in the lower limbs. The patient did not report painful or cold-aggravated myotonia, except for brief myotonia while swimming into cold water. The mother and a maternal aunt shared similar symptoms. He has taken topiramate with mild benefit, and then mexiletine with greater improvement. Neurological examination revealed handgrip myotonia with warm-up phenomenon and muscle hypertrophy, mainly in gluteal and quadriceps muscles, without any muscle weakness. The clinical phenotype was compatible with Thomsen disease. Interestingly, this mutation was recently found in another proband reporting mild symptoms and dominant inheritance (Lakraj *et al.* 2013).

Family 3. A c.1883T>C transition (L628P) was detected in a single male patient, now 6 years old and presenting at the age of 1 with quadriceps stiffness, in particular after prolonged immobilization and exacerbated by cold. The patient did not complain of painful myotonia. Neurological examination showed quadriceps and handgrip myotonia, with warm-up phenomenon; muscle strength was normal and lower limb muscle hypertrophy was observed. The mutation was compound heterozygous with the c.2434C>T transition (Q812X). No treatment was administered and the patient showed progression of myotonia during early infancy, suggesting a Becker phenotype.

Family 4. The c.1919T>G substitution (V640G) was identified in a male patient, now 54 years old, with onset during infancy characterized by lower limb stiffness and fatigability. Neurological examination over the years showed marked and diffuse muscle hypertrophy and myotonia, involving also facial and axial muscles, with warm-up phenomenon; in addition mild foot dorsiflexion weakness was detected. Myotonia was aggravated by cold and infections and was sometimes referred to as painful. Myotonia worsened over the years and the patient was given mexiletine and acetazolamide without any benefit. The clinical phenotype was suggestive of Becker myotonia and a second mutation was found (c.2680C>T; R894X). The father was reported to manifest with similar symptoms. None of the patients reported episodic transient weakness. Clinical data are summarized in Table 1.

Table 1. Clinical data for MC patients

Genotype	Exon/ Protein domain	Inheri- tance	Age of onset	Transient weakness	Muscle pain	Hyper- trophy	Cold effect	Warm- up	Clinical course	Phenotype	No. of Probands	Therapy
L198P	5/helix D	AD	8	No	No	Yes	No	Yes	Stable	Thomsen	1	Mex, effective
F484L	13/helix N	AD	18/20	No	No	Yes	No	Yes	Stable	Thomsen	2	Mex, effective
L628P (+ Q812X)	16/CBS1	AR	1	No	No	Yes	Worse	Yes	Worse	Becker	1	None
V640G (+ R894X)	16/CBS1	AR	Infancy	No	Yes	Yes	Worse	Yes	Worse	Becker	1	Mex and Actz ineffective

Mex, mexiletine; Actz, acetazolamide.

Electrophysiological characterization of dominant F484L MC mutation

The mutation F484L resides in the helix N that contributes to the chloride conductive pore (Fig. 1), and is dominantly inherited. In order to examine whether this mutation affected ClC-1 permeation and gating leading to muscle myotonia, we transfected tsA cells with equal amounts of wild-type or F484L cDNA (5 μg), and measured the *I–V* relationship and the overall apparent open probability by whole-cell patch clamp. Experiments were performed using a high intracellular chloride (134 mM) solution, to enhance current amplitude, or a more physiological low internal chloride (4 mM) solution.

In high intracellular chloride solution, F484L currents lacked the fast deactivation at negative potentials typical of wild-type ClC-1 currents, instead showing slow activation at each test potential till reaching a steady state (Fig. 2*A*). Instantaneous and steady-state current densities for F484L were greatly reduced at each voltage compared to WT (Fig. 2*B* and *C*; Table 2). As the currents of F484L showed strong outward rectification and did not saturate at positive potentials, the maximum current for normalization was arbitrarily taken at +180 mV to calculate the overall open probability. The voltage dependence of F484L activation appeared significantly shifted by about 150 mV towards positive potentials compared to WT channels (Fig. 2*D*; Table 2).

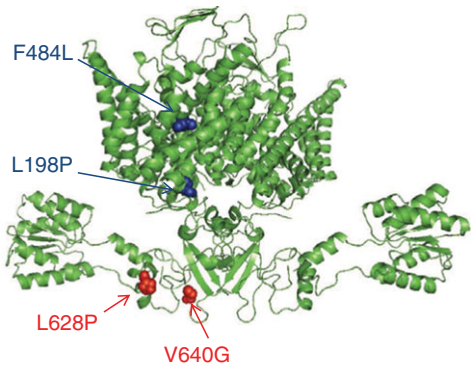

Figure 1. Three dimensional representation of hClC-1 channel
The representation is modelled upon the structure of CmClC showing the localization of the dominant and recessive MC mutations.

In low-chloride solution, F484L channels generated slowly activating and non-saturating currents at positive potentials, with kinetics evidently slower than those of WT channels (Fig. 3*A*). Steady-state current densities were smaller than WT in the range of physiological membrane potentials (Fig. 3*B*; Table 2). The voltage dependence of activation was, again, significantly right-shifted by about 130 mV compared to WT channels (Fig. 3*C*; Table 2). These results confirmed the biophysical changes measured in high-chloride solution for this mutant channel: due to its location inside the channel pore, the F484L mutation greatly disrupted ClC-1 channel kinetics and voltage dependence.

In order to gain deeper insight into the pathogenic mechanism behind this dominant mutation, we further analysed the effect of the F484L aminoacidic substitution on the fast and slow gating of the channel. Interestingly, separation of fast and common gating revealed that the voltage dependence for slow gating was greatly shifted in the positive direction for this mutation, so that F484L channels were less likely to be open in the physiological voltage range compared to WT (Fig. 4*A*; Table 3). Furthermore, the fast gating (fast gate closure) was practically eliminated by the F484L mutation, with an open probability of the fast gate of at least 0.8 at any given potential in high-chloride condition (Fig. 4*B*; Table 3).

To assess whether the dominant F484L mutation exerted the dominant-negative effect on WT subunits typical of mutations residing at the channel interface, we co-expressed F484L with equal amounts of WT cDNAs in tsA cells to recapitulate the heterozygous condition of patients. Interestingly, when co-expressed with WT in high-chloride conditions, F484L channels showed inwardly and outwardly rectifying whole-cell currents (Fig. 5*A* for WT+F484L). The current amplitude, at each voltage, was almost the sum of the currents of the respective homomeric channels (Fig. 5*B* and *C* for WT+F484L). For this heteromeric channel, the total P_o was shifted in the positive direction and was reduced at resting potentials compared to WT homomers but was greater than the P_o measured for the respective homomeric mutants (Fig. 5*D* for WT+F484L; Table 4). Therefore, the analysis of current level and open probability for WT+F484L heteromers revealed a phenotype in between that of the respective homomers, suggesting the presence

of at least two distinct populations of channels, rather than a dominant-negative effect.

Molecular dynamics simulations of WT and F484L channels

A preliminary visual inspection of the human ClC-1 homology model revealed that the dominant mutation F484L (helix N) is spatially located close to E232 (helix F) and Y578 (helix R), two residues recently proposed to contribute to voltage-dependent slow gating of the channel (Fig. 6; Bennetts & Parker, 2013). Such a domain (hereafter referred to as EY) behaves as a molecular gate whose action depends on the chance that a hydrogen bond (H-bond) interaction can take place between the side-chain of E232 (H-bond acceptor) and the side-chain of Y578 (H-bond donor) (Bennetts & Parker, 2013). When such an

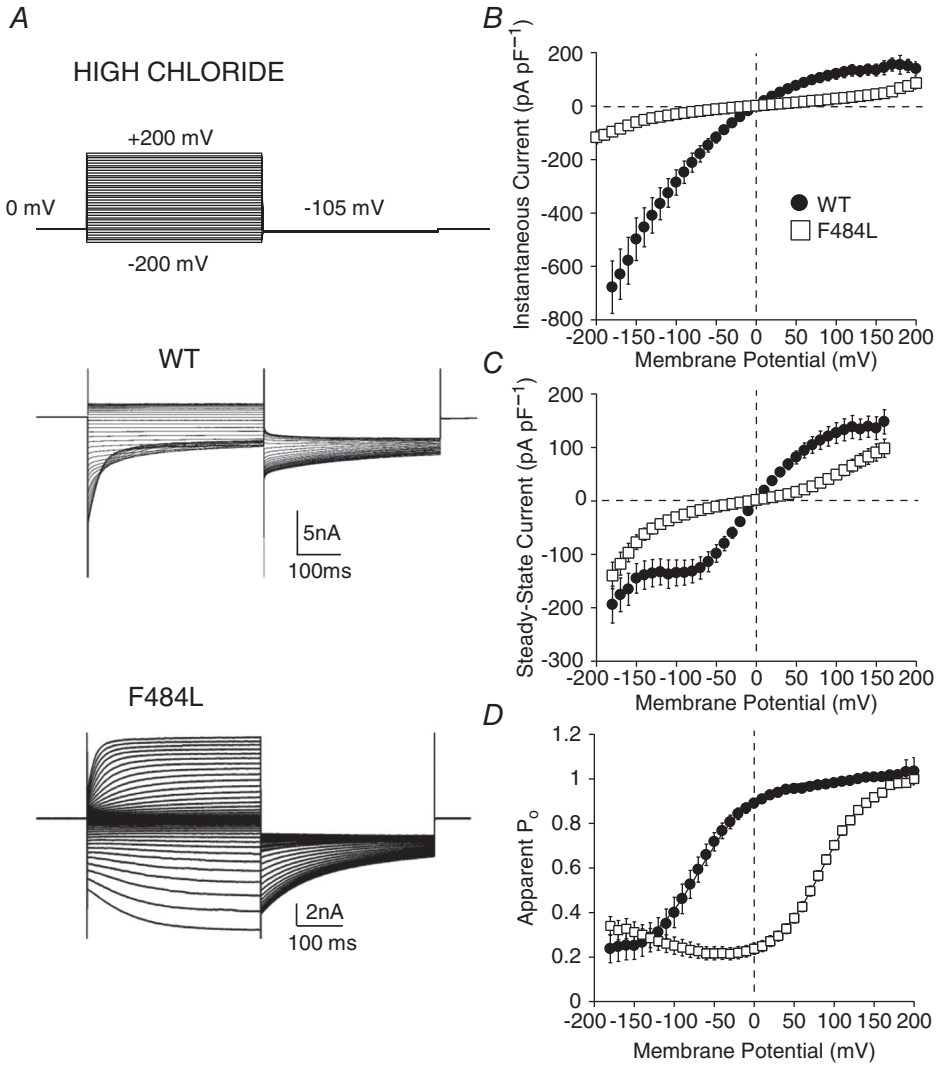

Figure 2. Functional characteristics of WT and F484L hClC-1 channels in high intracellular chloride
A, representative chloride currents recorded from tsA cells transfected with hClC-1 WT and F484L variants. Cells were held at 0 mV and 400 ms voltage pulses were applied from −200 to +200 mV in 10 mV intervals every 3 s. Mutant channels displayed different kinetics and reduced amplitude compared to WT. *B*, the instantaneous currents were measured at the beginning of test voltage pulses, normalized with respect to cell capacitance (pA pF^{-1}), and reported as a function of voltage. The F484L mutant does not show the strong inward rectification typical of WT channels. *C*, steady-state currents were measured at the end of test voltage pulses and reported as mean current density ± SEM in function of voltage. The F484L mutant generated reduced current densities with respect to WT. *D*, the voltage dependence of activation was determined by plotting the apparent open probability (P_o), calculated from tail currents measured at −105 mV, as a function of test voltage pulses. The relationships obtained from averaged data were fitted with a Boltzmann equation, and fit parameters are reported in Table 2. The mutant channels displayed a positively shifted voltage dependence of activation. Each point is the mean ± SEM from 6 to 14 cells.

Table 2. Biophysical parameters of hClC-1 WT and MC mutants

ClC-1	[Cl⁻] (mM)	$V_{0.5}$ (mV)	k (mV)	P_{min} (−90 mV)	IC (−60 mV) (pA pF^{-1})	SSC (+60 mV) (pA pF^{-1})	n cells
WT	134	−67 ± 1	33 ± 1	0.46 ± 0.06	−147 ± 25	94 ± 14	14
F484L	134	86 ± 1*	28 ± 1	0.24 ± 0.04*	−15 ± 4*	22 ± 4*	14
L198P	134	74 ± 1*	40 ± 0.4	0.05 ± 0.01*	−24 ± 8*	18 ± 6*	10
V640G	134	−47 ± 2	41 ± 2	0.38 ± 0.06	−61 ± 24	23 ± 11	8
L628P	134	−54 ± 1	28 ± 1	0.33 ± 0.04	−182 ± 63	90 ± 31	9
WT	4	−23 ± 2	43 ± 1	0.24 ± 0.03	—	360 ± 156	6
F484L	4	82 ± 8*	40 ± 3	0.25 ± 0.06	—	59 ± 12*	6
L198P	4	102 ± 2*	50 ± 1	0.09 ± 0.01*	—	48 ± 20*	6
L628P	4	−23 ± 1	28 ± 1	0.12 ± 0.03	—	338 ± 39	8

IC, instantaneous current; SSC, steady-state current; *$P < 0.05$ or less compared to WT.

interaction occurs, the passage of Cl^- is strongly hindered. In addition, the hClC-1 homology model shows that the residue F484 is engaged in π–π stacking interactions with two aromatic residues, namely F279 and F488 in the helices G and N.

Building on this evidence, in order to provide a putative molecular explanation for the positive shift of ClC-1 slow gating induced by the F484L, we carried out an in-depth analysis of the MD trajectories obtained for WT and F484L channels. In particular, we analysed the H-bond interactions occurring in the ClC-1 monomers in order to investigate the diverse behaviours of WT and F484L. An atom donor (A_D)–atom acceptor (A_A) distance equal to 4 Å and an angle A_D–H–A_A equal to 160 deg were used as thresholds to define the presence of the H-bond. Interestingly, the sole appreciable

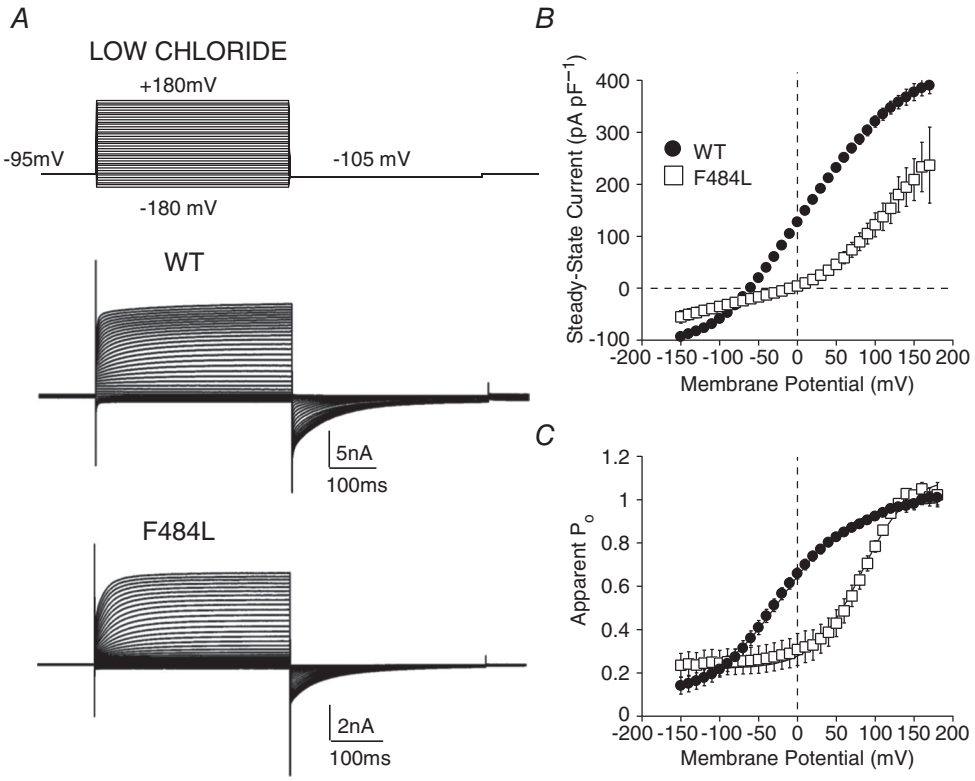

Figure 3. Functional characteristics of WT and F484L hClC-1 channels in low intracellular chloride
A, chloride currents were recorded in tsA cells transfected with WT and F484L hClC-1 variants. Cells were held at −95 mV and 400 ms voltage pulses were applied from −180 to +180 mV in 10 mV intervals every 3 s. Mutant chloride currents displayed slower kinetics of activation compared to WT. *B*, the steady-state current density–voltage relationships were drawn as in Fig. 2*C*. *C*, the voltage dependence of activation, determined as in Fig. 2*D*, was fitted with a Boltzmann function. Fit parameters are reported in Table 2. The F484L mutant channels displayed a positively shifted voltage dependence. Each point is the mean ± SEM from 6 to 14 cells.

Table 3. Channel open probability for slow gating ($P_{o,slow}$) and fast gating ($P_{o,fast}$) for WT and MC hClC-1 mutants

ClC-1	$V_{0.5}$ $P_{o,slow}$ (mV)	k (mV)	P_{min} (−90 mV)	$V_{0.5}$ $P_{o,fast}$ (mV)	k (mV)	P_{min} (−90 mV)	n cells
WT	−78 ± 1	35 ± 1	0.68 ± 0.05	−91 ± 1	23 ± 1	0.82 ± 0.1	8
F484L	111 ± 3*	33 ± 2	0.26 ± 0.05*	—	—	—	6
L198P	53 ± 1*	38 ± 1	0.18 ± 0.01*	−38 ± 2	54 ± 2	0.7 ± 0.1	5
V640G	−49 ± 4	46 ± 3	0.56 ± 0.02	−69 ± 1	27 ± 1	0.61 ± 0.1	4
L628P	−69 ± 1	18 ± 1	0.68 ± 0.03	−87 ± 1	30 ± 1	0.65 ± 0.05	6

*$P < 0.05$ or less compared to WT.

Table 4. Biophysical parameters of heteromeric WT+F484L and WT+L198P channels

ClC-1	$[Cl^-]$ (mM)	$V_{0.5}$ (mV)	k (mV)	P_{min} (−90 mV)	IC (−60 mV) (pA pF^{-1})	SSC (+60 mV) (pA pF^{-1})	n cells
WT+F484L	134	−63 ± 3 69 ± 7	41 ± 3 29 ± 6	0.46 ± 0.04	−273 ± 64	220 ± 49	7
WT+L198P	134	−61 ± 1 58 ± 1	26 ± 1 39 ± 1	0.23 ± 0.03	−177 ± 68	140 ± 51	6

IC, instantaneous current; SSC, steady-state current.

difference between the mutants was the above-described H-bond interaction between E232 and Y578. Importantly, in the simulation timescales considered in our analysis the H-bond formation is very frequently observed in both F484L monomers (11.04% and 47.30% rate of occurrence for monomers A and B, respectively), whereas it is significantly reduced in WT (0.05% and 1.90% rate of occurrence for monomers A and B, respectively) in the considered time of simulation (20 ns). In other words, the H-bond is immediately lost during the MD simulations of WT, although it is present in the described initial hClC-1 homology model (Fig. 6). In contrast, the replacement of F484 with the pathogenic leucine residue (F484L) triggers the EY closure in both the monomers, thus indicating that the gating mechanism is operated through the remote control of the single residue at position 484.

This difference in behaviour between WT and F484L is also clearly confirmed by the time dependence of the distance between the H-bond donor and H-bond acceptor side-chain atoms of the Y578 and E232 interaction (hereafter referred to as $d_{EY;}$ Fig. 7*A* and *B*). As shown in Fig. 7, d_{EY} can switch from an average value of 5 Å (open state) to 3 Å (closed state) for both WT and F484L mutants. However, the closed conformation occurs at a low probability for WT, and, whenever it happens, the transition back to the open state is extremely fast.

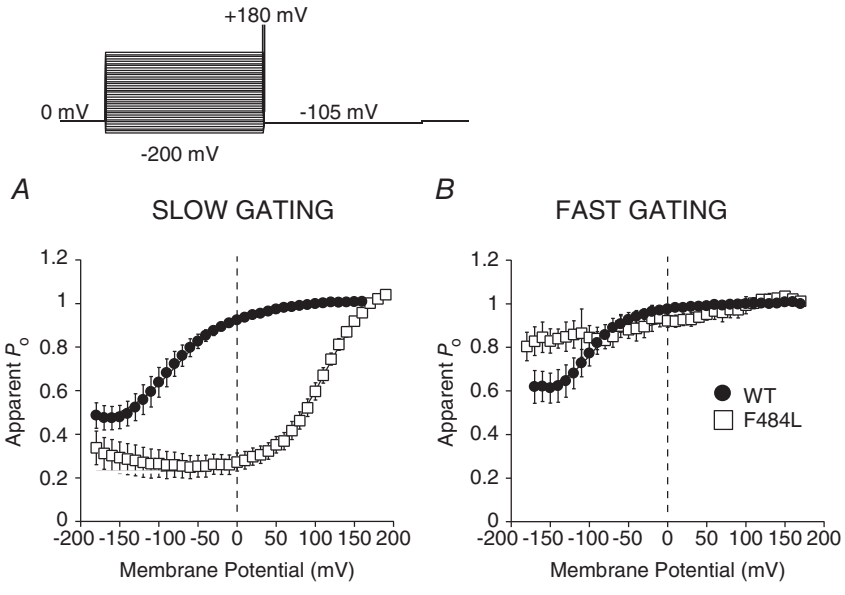

Figure 4. Apparent open probabilities for fast and slow gating of WT and F484L hClC-1 channels
Apparent open probabilities for slow (*A*) and fast gating (*B*) in mutant F484L compared to WT. Open probability for slow gating was obtained as described in the Methods section. Open probability of the fast gates was calculated for a given test voltage by dividing the relevant total P_o by its corresponding $P_{o,slow}$. The substantial positive shifts in overall P_o for F484L shown in Fig. 2 was mainly due to a large positive shift in $P_{o,slow}$. For each channel, $n = 6$–8 cells. Fit parameters are reported in Table 3.

Importantly, monomer A remains in the open state during the entire simulation. The transition to the closed state is, instead, more often observed in F484L (both the monomers display this transition within the total simulation time) and is even more stable at least on the timescale of 20 ns.

Taken together, these observations would suggest that the aromatic residue F484 is a key element of the slow gating mechanism in WT channels. Furthermore, its mutation, as in F484L, is responsible for the positive shift of the voltage dependence of the slow gate as a result of the higher frequency and stability of the H-bond formation between E232 and Y578.

Electrophysiological characterization of other MC mutations

Among previously identified mutations, we decided to characterize, using patch-clamp electrophysiology, the dominant mutation L198P located in the helix D, a pore region comprising the chloride binding sites, and the recessive mutations V640G and L628P residing in the CBS1 domain (Fig. 1; Brugnoni *et al.* 2013; Lakraj *et al.* 2013).

In high-chloride solution, L198P channels conducted very little current at negative potentials and very slowly activating currents at positive potentials (Fig. 8*A*), with instantaneous and steady-state current densities greatly reduced compared to WT (Fig. 8*B* and *C*; Table 2). Similarly, instantaneous and steady-state current amplitudes were greatly reduced for V640G channels compared to WT (Fig. 8*B* and *C*; Table 2). Conversely, L628P showed current kinetics and densities similar to WT (Fig. 8*A*–*C*; Table 2).

The voltage dependence of L198P activation appeared significantly shifted by about 150 mV towards positive potentials compared to WT channels (Fig. 8*D*; Table 2), implying that this mutant channel was almost closed at voltages near the skeletal muscle resting potential (Table 2). In contrast, the analysis of the apparent open probability revealed no significant differences for the V640G and L628P mid-activation voltages with respect to WT (Fig. 8*D*; Table 2).

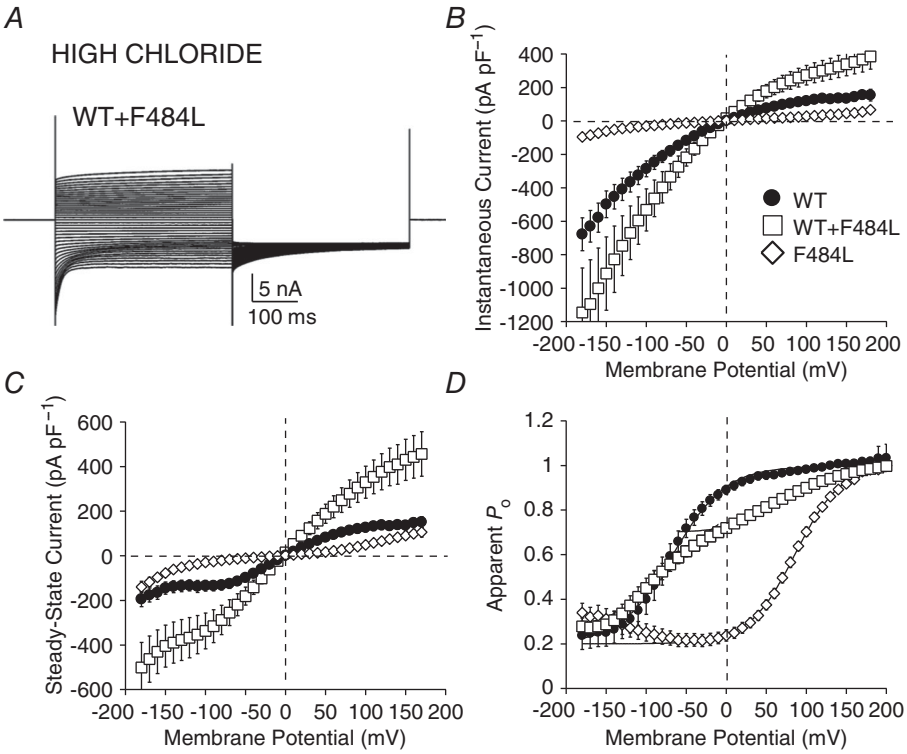

Figure 5. Functional characteristics of heteromeric WT+F484L hClC-1 channels in high intracellular chloride

A, representative current traces elicited from tsA cells co-transfected with equal amount of WT and F484L cDNAs in high intracellular chloride. *B*, the instantaneous currents in high intracellular chloride were measured as in Fig. 2*B*, for WT, F484L and WT+F484L channels. *C*, steady-state currents in high intracellular chloride were measured as described in Fig. 2*C*. *D*, the voltage dependence of activations, determined as in Fig. 2*D*, were fitted with a double Boltzmann function. Fit parameters are reported in Table 4. The heteromeric channels displayed a positively shifted voltage dependence compared to WT. Each point is the mean ± SEM from 7 cells.

In low-chloride solution, L198P channels generated slowly activating and non-saturating currents at positive potentials, with kinetics slower than those of WT channels (Fig. 9*A*). The steady-state current densities were smaller (Fig. 9*B*; Table 2) and the voltage dependence of activation was, again, significantly right-shifted by about 130 mV, compared to WT channels (Fig. 9*C*; Table 2). The L628P channels generated slowly activating and saturating currents at positive potentials, with steady-state current densities and voltage dependence of activation similar to WT in the range of physiological membrane potentials (Fig. 9*A*–*C*; Table 2), thus further questioning mutant pathogenicity. Chloride currents generated by V640G were too small to allow satisfactory biophysical analysis in low-chloride solution.

In order to further assess the contribution of these residues to channel gating, we analysed the effect of the L198P, V640G and L628P mutations on the open probability of the fast and slow gating using whole-cell patch clamp. Interestingly, the voltage dependence of slow gating for L198P was greatly shifted in the positive direction (Fig. 10*A*; Table 3). In contrast, the open probabilities for fast and slow gating were not significantly different in V640G and L628P compared to WT channels (Fig. 10*A* and *B*; Table 3).

Similar to F484L, in the presence of high intracellular chloride, the L198P pore mutant subunit did not exert a measureable dominant negative effect on WT in co-expression experiments (Fig. 10*C* for WT+L198P). The current amplitude, at each voltage, was almost the sum of the currents of the respective homomeric channels (Fig. 10*D* and *E* for WT+L198P), and the total P_o was almost intermediate between that measured for the respective homomeric channels (Fig. 10*F* for WT+L198P; Table 4).

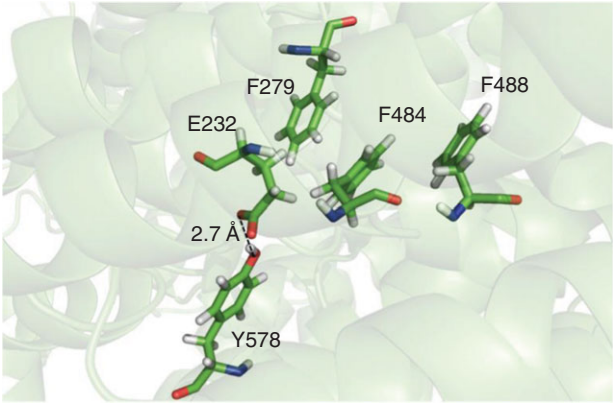

Figure 6. Zoom of the CmClC-based hClC-1 homology model used in the present study
Important residues are shown as sticks and the H-bond between E232 and Y578 is shown as dashed line.

Discussion

Here we report a thorough characterization of the ClC-1 myotonic mutation F484L, which is located outside the known 'hot spot' for dominant MC mutations (Fialho *et al.* 2007), and results in a Thomsen phenotype (Brugnoni *et al.* 2013). Satisfactorily, the analysis of MD trajectories highlighted the key action of this phenylalanine at position 484 in controlling the slow gating of ClC-1. We also describe the functional consequences of three other ClC-1 mutations associated to peculiar myotonic phenotypes, and residing on domains relevant for channel function (Brugnoni *et al.* 2013).

Effect of F484L mutation on hClC-1 channel gating

In order to disclose novel pathogenic mechanisms for MC and, in parallel, to clarify the structural requirements for channel gating, we used patch-clamp electrophysiology and molecular dynamics simulations to characterize the dominant F484L mutation. Here we show that, when expressed in mammalian cells lines, this mutation, located in the ion conducting pore, drastically reduces chloride current at physiological potentials but does not reveal a dominant-negative effect on WT in co-expression experiments. As most dominant mutations, the shift of the voltage dependence of the channel slow gating to very positive potentials mainly accounts for the observed reduction of chloride current.

The most interesting and novel finding of this study is the key role of the F484L mutation in ClC-1 gating. While it has been ascertained that the carboxyl side-chain of the glutamate residue E232 of helix F is the main domain responsible for fast gating, the molecular determinants of the slow gate are still awaiting elucidation (Dutzler *et al.* 2002, 2003). Emerging evidence supports the idea that slow gating results from complex conformational rearrangements involving the fast gate E232 and the C-terminal domains via helix R, besides the boundary helices between the two protopores typically known to take part to this gating process (Duffield *et al.* 2003; Estevez *et al.* 2004; Cederholm *et al.* 2010; Feng *et al.* 2010; Ma *et al.* 2011; Bennetts & Parker, 2013; Stölting *et al.* 2014*a*).

We chose to investigate further the molecular mechanism behind the right-shift in the voltage dependence of the slow gate measured in the electrophysiological experiments for F484L channels, on the basis of the close proximity of F484 (helix N) to E232 (helix F) and Y578 (helix R) (Bennetts & Parker, 2013). Interestingly, these latter residues have been proposed to establish an H-bond with their charged side-chains that is required for the slow gating of ClC-1 channels (Bennetts & Parker, 2013). Thus, we used MD simulations to assess the contribution of the residue F484L to the H-bond formation between E232 and Y578. According to our clear-cut interpretive

hypothesis, the presence of this highly conserved aromatic residue allows the formation of the H-bond between E232 and Y578 at a low rate compatible with the physiological activity of the ClC-1 channel. Indeed, in WT channels, the side-chain of E232 establishes an H-bond interaction with F484. Such an interaction occurs after a conformational rearrangement of the side-chain of E232 and the consequent disruption/weakening of its H-bond with Y578. The H-bond between F484 and E232 is guaranteed by the π–π stacking interactions between F484 and two close aromatic residues (F279 and F488) and is even strengthened by an additional H-bond involving the backbones of F484 and F488 (Fig. 7*C*). Remarkably, in myotonic patients carrying the F484L mutation, the replacement of the aromatic phenylalanine with the aliphatic leucine disrupts the aromatic sandwich-like conformation (observed for F488) that, accordingly, confers a higher conformational flexibility (see the arrow in Fig. 7), which determines the breaking of the H-bond between the backbone of F484 and that of F488. This event induces different conformational changes in the backbone of the residue at position 484 with the effect of weakening the chance of interaction with E232. In turn, this will increase the rate of occurrence of the H-bond formation between E232 and Y578, strengthening the stability of the slow gate in its closed state.

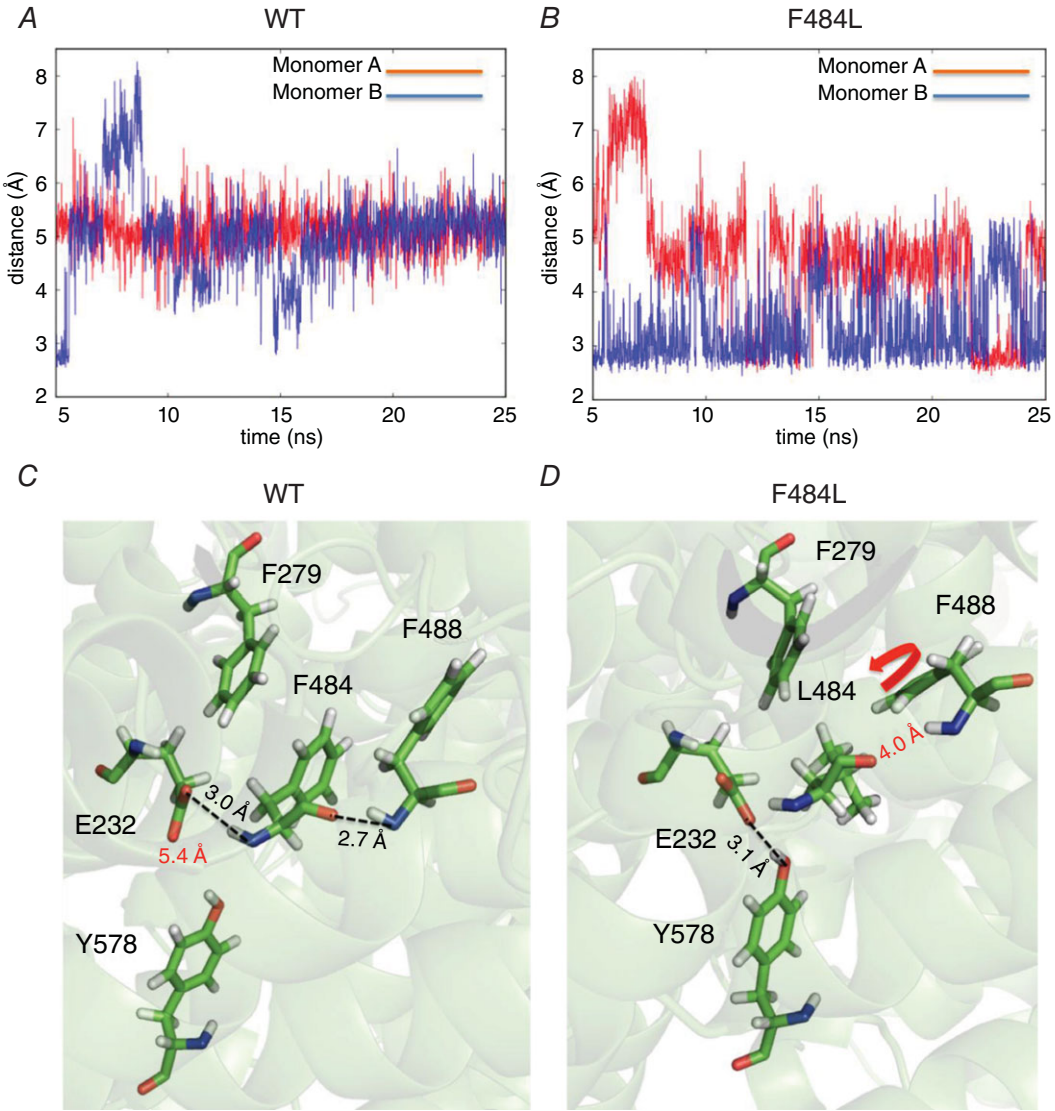

Figure 7. Analysis of hydrogen bond interactions occurring in WT and F484L dimers
A and *B*, time-dependent evolutions of the distance between the oxygen donor of Y578 side-chain and the nearest oxygen acceptor of E232 $^{\text{side-chain}}$, for WT and F484L channels. The results computed for both the two monomers (*A* and *B*) are presented. *C* and *D*, selected frames showing the different H-bond interactions established in WT and F484L in the EY domain. Important residues are shown as sticks while the H-bond interactions are depicted by a dashed line.

There are no compounds that directly open ClC-1, whereas a few compounds are known to block the channel unselectively (Pusch *et al.* 2002). Importantly, mutations of the residue F484 were reported to affect the binding of ClC-1 inhibitors (Estevez *et al.* 2003). Therefore, the optimization of these lead compounds together with an understanding of the exact gating defect underlying specific mutant channels would pave the way (Alberga *et al.* 2014; Mangiatordi *et al.* 2015) to the development of drugs acting specifically on mutant ClC-1 channels. Hypothetically, we expect that any drug binding inside the pore and bearing an aromatic moiety able to restore the above-described π–π stacking interactions would reverse the positive shift in the slow gate, thereby representing a possible specific therapy for F484L carriers.

Genotype–phenotype correlation

In order to correlate different degrees of myotonic symptoms to different effects of ClC-1 mutations on channel function, we performed a detailed clinical evaluation of MC patients in parallel with the functional analysis of mutant channels.

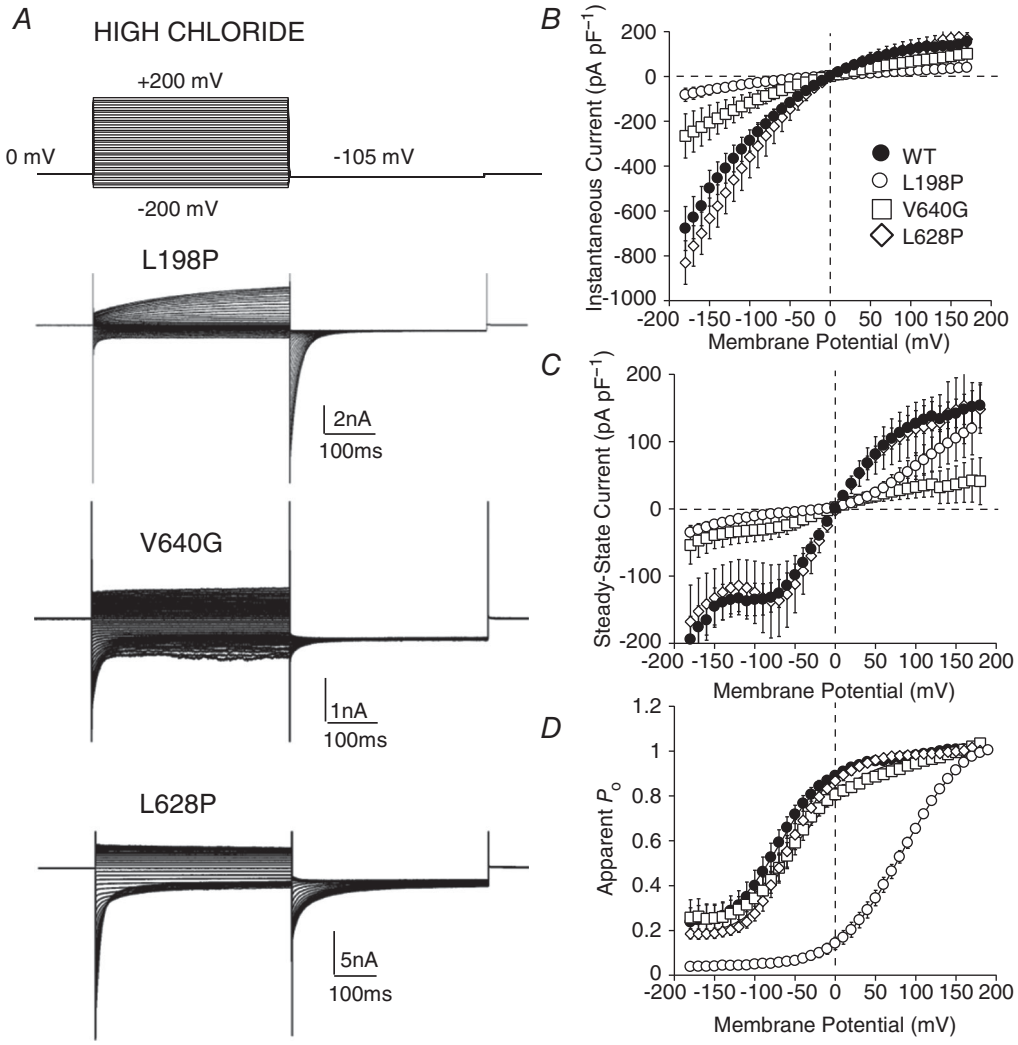

Figure 8. Functional characteristics of L198P, V640G and L628P hClC-1 channels in high intracellular chloride

A, representative whole-cell current traces elicited from tsA cells transfected with the dominant L198P and recessive variants V640G or L628P. Cells were held at 0 mV and 400 ms voltage pulses were applied from −200 to +200 mV in 10 mV intervals every 3 s. Mutant channels displayed similar kinetics compared to WT. *B*, the instantaneous currents were measured as in Fig. 2*B* for WT, L198P, V640G and L628P. *C*, steady-state currents were measured as described in Fig. 2*C*. L198P and V640G generated reduced current densities with respect to WT. *D*, the voltage dependence of activation, determined as in Fig. 2*D*, was fitted with a Boltzmann function. Fit parameters are reported in Table 2. The activation curve for V640G and L628P was similar to the WT curve while that of L198P was severely right-shifted. Each point is the mean ± SEM from 8–9 cells.

The neurological examination of the patients carrying the F484L mutation revealed a mild Thomsen phenotype associated with a stable clinical course, without transient weakness, cold-aggravated or painful myotonia. When expressed in tsA cells, this mutant channel showed not only severely reduced chloride currents, but also modified gating compared to WT channel. Interestingly, co-expression of F484L with WT, which was expected to mimic the heterozygous condition of affected patients, failed to show any evidence of dominant-negative effect. Collectively, the positive shift of the overall open probability as well as the reduction in chloride conductance observed in the patch-clamp experiments might be sufficient to recapitulate the mild clinical phenotype of this case of dominantly inherited MC.

Remarkably, the lack of negative interactions between mutant and WT subunits implies that dominant MC mutations residing in helices lining the channel pore might cause myotonia with a molecular mechanism different from that of mutations residing within the intra-membrane dimerization interface. That is, our data strongly suggest that the dominant-negative effect of a mutant on the WT subunit is not a compulsory condition for the etiopathology of dominant myotonia congenita in the cases of pore mutations, with a huge shift of slow gating of mutant pore being sufficient to cause a mild myotonic phenotype.

These experimental data are also in agreement with the results of a recent study correlating the molecular pathogenesis of MC to the position of dominant and recessive MC mutations on the hClC-1 channel, using the crystallographic structure of CmCLC (Feng *et al.* 2010; Skalova *et al.* 2013). Most dominant MC mutations proven to cause a dominant-negative effect when co-expressed with WT subunits effectively reside at the boundary region between two monomers or in its proximity. Conversely, mutations occurring in the channel pore show no dominant-negative effect and can cause the disease by other mechanisms (Skalova *et al.* 2013).

It is worth noting that we cannot definitely rule out the possibility of specific behaviour of the mutant in the muscle fibre context (e.g. different allele expression) or the presence of a yet-unidentified mutation in the *CLCN1* gene not detectable with custom genetic screening techniques (Zhang *et al.* 1996; Raya Rayan *et al.* 2012; Richman *et al.* 2012; Ulzi *et al.* 2014). Studies of more families with similar

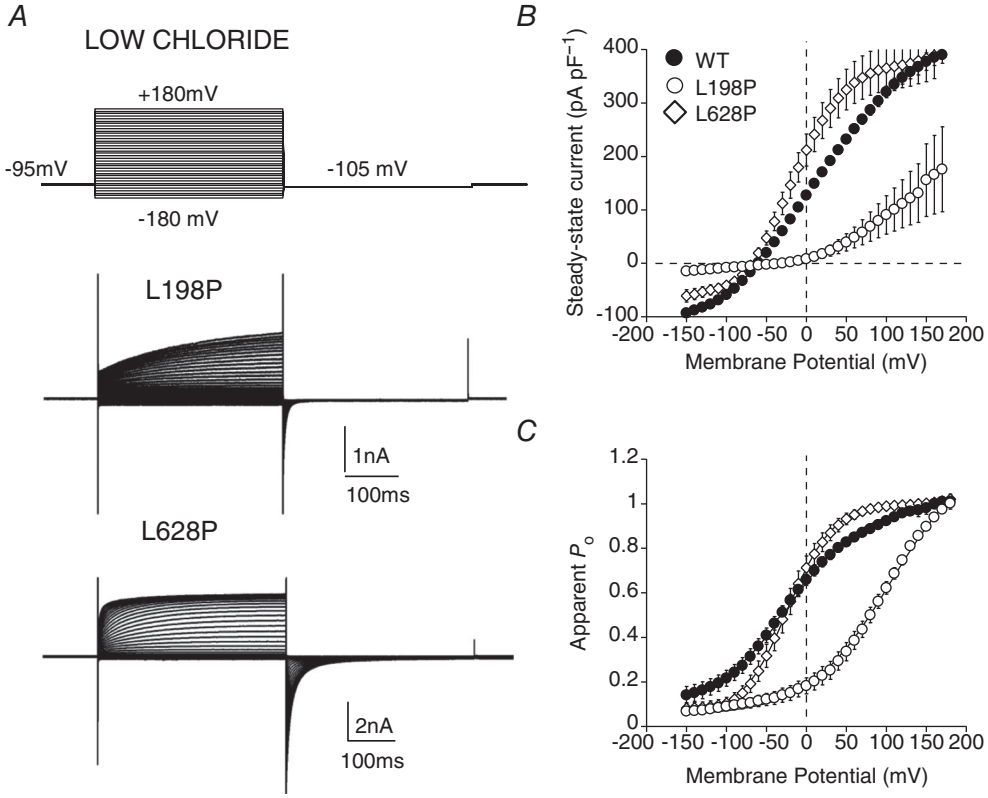

Figure 9. Functional characteristics of L198P and L628P hClC-1 channels in low intracellular chloride
A, chloride currents were recorded in tsA cells transfected with L198P and L628P variant. Cells were held at −95 mV and 400 ms voltage pulses were applied from −180 to +180 mV in 10 mV intervals every 3 s. *B*, the steady-state current density–voltage relationships were drawn as in Fig. 2*C* for WT, L198P and L628P. *C*, the voltage dependence of activation, determined as in Fig. 2*D*, was fitted with a Boltzmann function. Fit parameters are reported in Table 2. Each point is the mean ± SEM from 8 cells.

dominant mutations and recordings from patients' muscle biopsies would be helpful to confirm our hypothesis.

To support this hypothesis, we thus performed an electrophysiological characterization of another pore mutation, L198P, associated with a Thomsen phenotype. Similarly to F484L, we found that L198P mutant subunits are almost closed at physiological membrane potentials due to a large shift of the open probability of the voltage-dependent slow gating, and do not exert a dominant-negative effect when co-expressed with unaffected subunits. Interestingly, the L198P mutation is located in helix D, which forms part of the ion conductive pore and is known to interact with helices H, R and the CBS2 domain, notably being involved in the mechanism of slow gating (Bennetts & Parker, 2013; Skalova *et al.* 2013). Two other substitutions have been found at the same conserved position in myotonic patients (Simpson *et al.* 2004; Brugnoni *et al.* 2013). Thus, these evidences suggest

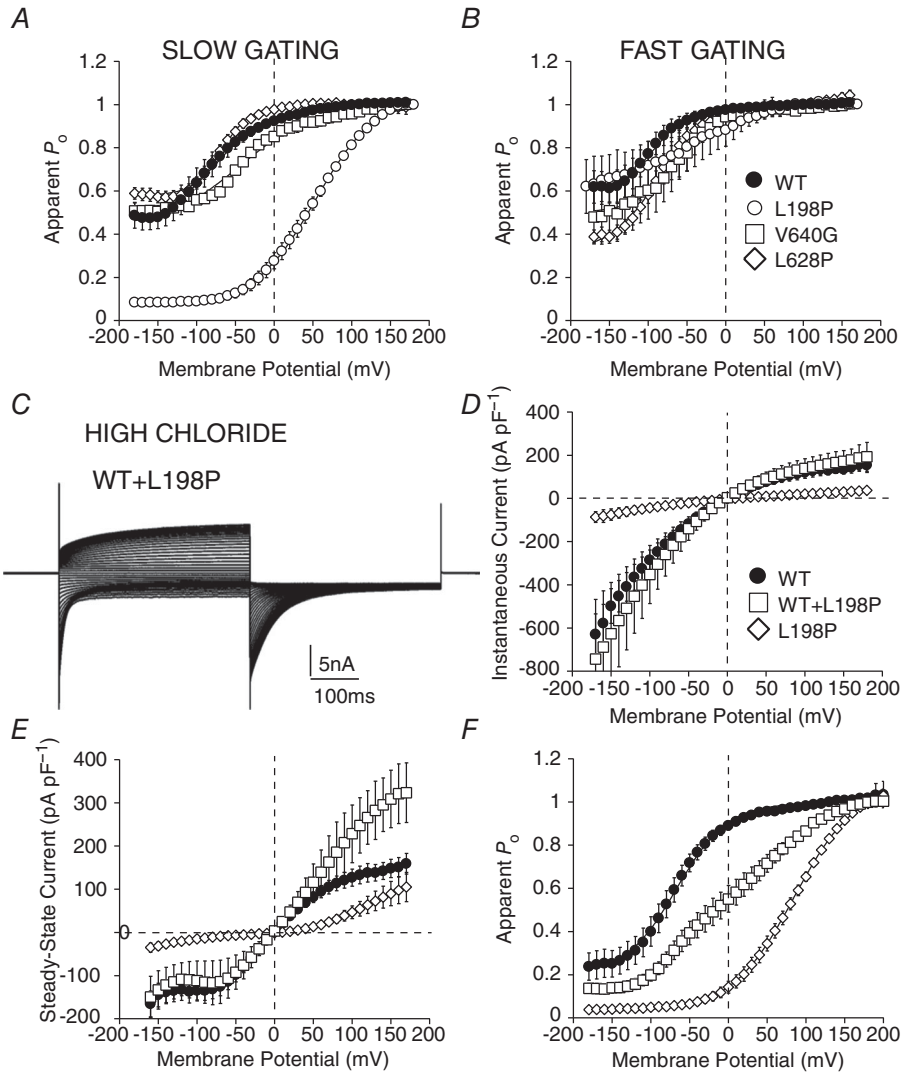

Figure 10. Open probabilities for fast and slow gating of WT, L198P, V640G and L628P hClC-1 channels, and functional characteristics of heteromeric WT+L198P hClC-1 channels
Apparent open probabilities for slow (*A*) and fast (*B*) gating in mutants L198P, V640G and L628P compared to WT. Open probability for common gating ($P_{o,slow}$) was obtained as described in the Methods section. Open probability of the fast gates ($P_{o,fast}$) was calculated for a given test voltage by dividing the relevant P_o by its corresponding $P_{o,slow}$. For each channel, $n = 4$–6 cells. Fit parameters are reported in Table 3. *C*, representative current traces elicited from tsA cells co-transfected with equal amounts of WT and L198P cDNAs in high intracellular chloride. *D*, the instantaneous currents in high intracellular chloride were measured as in Fig. 8*B*, for WT, L198P and WT+L198P channels. *E*, steady-state currents in high intracellular chloride were measured as described in Fig. 8*C*. *F*, the voltage dependence of activations, determined as in Fig. 8*D*, were fitted with a double Boltzmann function. Fit parameters are reported in Table 4. The heteromeric channels displayed a positively shifted voltage dependence compared to WT. Each point is the mean ± SEM from 6 cells.

that this spot on helix D is remarkable for disease aetiology, ion permeability and gating. An in-depth characterization would be of help to verify whether the substitution of L198 with the smaller and more rigid proline may result in an empty space in the helix D, probably disturbing interactions with nearby helices and increasing the stability of the slow gate, as shown for F484L.

In addition, we studied two recessive mutations, L628P and V640G, located close to the intracellular CBS domains of ClC-1. V640G is associated with a very severe form of MC mainly characterized by marked and diffuse muscle hypertrophy and myotonia, involving all muscles, with relevant progression over the years. Strikingly, myotonia was aggravated by cold and infections, sometimes reported as painful and did not benefit from the common symptomatic treatments. Consistently, the V640G channel expressed in tsA cells leads to drastically reduced channel activity in the plasma membrane as shown by its smaller current amplitude compared to WT. This mutation was found to be compound heterozygous with the truncating mutant R894X that causes reduced channel activity and enhanced degradation, and exerts a weak dominant-negative effect on wild-type currents (Meyer-Kleine *et al.* 1995; Duno *et al.* 2004; Macias *et al.* 2007; Papponen *et al.* 2008; Mazon *et al.* 2012). Therefore, one additional hypothesis for the occurrence of a severe Becker phenotype in patients carrying both R894X and V640G may be that the R894X exhausts V640G by enhancing the degradation of heterodimers, thereby reducing further the sarcolemma chloride conductance. Such a dramatic effect on channel expression may also provide a likely explanation for the lack of responsiveness of the affected patient to acetazolamide, a carbonic anhydrase inhibitor known to increase human ClC-1 open probability and alleviate MC clinical symptoms (Eguchi *et al.* 2006; Desaphy *et al.* 2013).

The mutation L628P was found in a patient with less severe myotonia than was shown by the V640G carrier, without muscle weakness and pain; however, the myotonia had a very early onset and worsened during infancy, suggesting a Becker phenotype. When expressed in tsA cells, the L628P mutant channel shows current amplitude and voltage dependence very similar to those of WT proteins, thus bringing its pathogenicity into question. Furthermore, the proband presented a compound heterozygous mutant, Q812X, that has not been functionally characterized, but, given its position in the ClC-1 sequence, might give rise to a truncated protein with reduced activity, as shown for other neighboring C-terminal variants (Macias *et al.* 2007; Ulzi *et al.* 2012; Richardson *et al.* 2014). Therefore, on one hand, the truncated mutants Q812X might alone explain the abnormal phenotype. On the other hand, we cannot rule out that L628P may harbour some hidden muscle-specific defects that would account for the recessive inheritance seen in patients with the mutation. Modifications occurring within the stretch between CBS1 and CBS2, for instance, might impair channel interaction with nucleotides, such as ATP and NAD^+, or regulatory proteins (Bennetts *et al.* 2007; Tseng *et al.* 2011; Bennetts *et al.* 2012). Alternatively, the L628P mutation might modify the phenotype caused by the co-existing MC mutation without being pathogenic by itself.

In conclusion, we demonstrate that mutations located in the channel pore associated with dominant myotonia with mild symptoms affect the gating mechanisms of ClC-1 channels but do not exert a dominant-negative effect on WT subunits. Through MD simulations, we highlight the pivotal role of the pore aromatic residue F484 in the molecular mechanism of slow gating mediated by E232 and Y578, further supporting the view that fast and slow gating are closely interrelated processes (Cederholm *et al.* 2010; Ma *et al.* 2011).

Moreover, our electrophysiological data suggest that mutations located in the CBS1 domain reduce channel density or carry muscle-specific defects, but have few implications for the gating processes of the channel.

A better understanding of the structure–function–phenotype correlation carried by different mutations in ClC-1 channels, through combined clinical, electrophysiology and molecular dynamics studies, represents an essential requirement in the development of personalized treatment for MC, which is to date only symptomatic.

References

Accardi A & Pusch M (2000). Fast and slow gating relaxations in the muscle chloride channel CLC-1. *J Gen Physiol* **116**, 433–444.

Adelman SA & Doll JD (2008). Generalized Langevin equation approach for atom/solid-surface scattering: General formulation for classical scattering off harmonic solids. *J Chem Phys* **64**, 2375–2388.

Alberga D, Nicolotti O, Lattanzi G, Nicchia GP, Frigeri A, Pisani F, Benfenati V & Mangiatordi GF (2014). A new gating site in human aquaporin-4: Insights from molecular dynamics simulations. *Biochim Biophys Acta* **1838**, 3052–3060.

Bennetts B & Parker MW (2013). Molecular determinants of common gating of a ClC chloride channel. *Nat Commun* **4**, 2507–2517.

Bennetts B, Parker MW & Cromer BA (2007). Inhibition of skeletal muscle ClC-1 chloride channels by low intracellular pH and ATP. *J Biol Chem* **282**, 32780–32791.

Bennetts B, Yu Y, Chen TY & Parker MW (2012). Intracellular β-nicotinamide adenine dinucleotide inhibits the skeletal muscle ClC-1 chloride channel. *J Biol Chem* **287**, 25808–25820.

Brugnoni R, Galantini S, Confalonieri P, Balestrini MR, Cornelio F & Mantegazza R (1999). Identification of three novel mutations in the major human skeletal muscle chloride channel gene (CLCN1), causing myotonia congenita. *Hum Mutat* **14**, 447.

Brugnoni R, Kapetis D, Imbrici P, Pessia M, Canioni E, Colleoni L, Kerlero de Rosbo N, Morandi L, Cudia P, Gashemi N *et al.* (2013). A large cohort of myotonia congenita probands: novel mutations and a high-frequency mutation region in exons 4 and 5 of the CLCN1 gene. *J Hum Genet* **58**, 581–587.

Burge JA & Hanna MG (2012). Novel insights into the pathomechanisms of skeletal muscle channelopathies. *Curr Neurol Neurosci Rep* **12**, 62–69.

Cederholm JM, Rychkov GY, Bagley CJ & Bretag AH (2010). Inter-subunit communication and fast gate integrity are important for common gating in hClC-1. *Int J Biochem Cell Biol* **42**, 1182–1188.

Colding-Jørgensen E (2005). Phenotypic variability in myotonia congenita. *Muscle Nerve* **32**, 19–34.

Darden T, York D & Pedersen L (1993). Particle mesh Ewald: An N-log(N) method for Ewald sums in large systems. *J Chem Phys* **98**, 10089–10092.

Desaphy J-F, Gramegna G, Altamura C, Dinardo MM, Imbrici P, George AL Jr, Modoni A, LoMonaco M & Conte Camerino D (2013). Functional characterization of ClC-1 mutations from patients affected by recessive myotonia congenita presenting with different clinical phenotypes. *Exp Neurol* **248**, 530–540.

Duffield M, Rychkov G, Bretag A & Roberts M (2003). Involvement of helices at the dimer interface in ClC-1 common gating. *J Gen Physiol* **121**, 149–161.

Duno M, Colding-Jorgensen E, Grunnet M, Jespersen T, Vissing J & Schwartz M (2004). Difference in allelic expression of the CLCN1 gene and the possible influence on the myotonia congenita phenotype. *Eur J Hum Genet* **12**, 738–743.

Dutzler R (2006). The ClC family of chloride channels and transporters. *Curr Opin Struct Biol* **16**, 439–446.

Dutzler R, Campbell EB, Cadene M, Chait BT & MacKinnon R (2002). X-ray structure of a ClC chloride channel at 3.0 A reveals the molecular basis of anion selectivity. *Nature* **415**, 287–294.

Dutzler R, Campbell EB & MacKinnon R (2003). Gating the selectivity filter in ClC chloride channels. *Science* **300**, 108–112.

Eguchi H, Tsujino A, Kaibara M, Hayashi H, Shirabe S, Taniyama K & Eguchi K (2006). Acetazolamide acts directly on the human skeletal muscle chloride channel. *Muscle Nerve* **34**, 292–297.

Estévez R, Pusch M, Ferrer-Costa C, Orozco M & Jentsch TJ (2004). Functional and structural conservation of CBS domains from CLC chloride channels. *J Physiol* **557**, 363–378.

Estévez R, Schroeder BC, Accardi A, Jentsch TJ & Pusch M (2003). Conservation of chloride channel structure revealed by an inhibitor binding site in ClC-1. *Neuron* **38**, 47–59.

Feng L, Campbell EB, Hsiung Y & MacKinnon R (2010). Structure of a eukaryotic CLC transporter defines an intermediate state in the transport cycle. *Science* **330**, 635–641.

Fialho D, Schorge S, Pucovska U, Davies NP, Labrum R, Haworth A, Stanley E, Sud R, Wakeling W, Davis MB, Kullmann DM & Hanna MG (2007). Chloride channel myotonia: exon 8 hot-spot for dominant-negative interactions. *Brain* **130**, 3265–3274

Fournier E, Viala K, Gervais H, Sternberg D, Arzel-Hézode M, Laforêt P, Eymard B, Tabti N, Willer JC, Vial C & Fontaine B (2006) Cold extends electromyography distinction between ion channel mutations causing myotonia. *Ann Neurol* **60**, 356–365.

George AL Jr, Crackower MA, Abdalla JA, Hudson AJ & Ebers GC (1993). Molecular basis of Thomsen's disease (autosomal dominant myotonia congenita) *Nat Genet* **3**, 305–310.

Griggs RC, Moxley RT III, Riggs JE & Engel WK (1978). Effects of acetazolamide on myotonia. *Ann Neurol* **3**, 531–537.

Ha K, Kim SY, Hong C, Myeong J, Shin JH, Kim DS, Jeon JH & So I (2014). Electrophysiological characteristics of six mutations in hClC-1 of Korean patients with myotonia congenita. *Mol Cells* **37**, 202–212.

Horga A, Raja Rayan DL, Matthews E, Sud R, Fialho D, Durran SC, Burge JA, Portaro S, Davis MB, Haworth A & Hanna MG (2013) Prevalence study of genetically defined skeletal muscle channelopathies in England. *Neurology* **80**, 1472–1475.

Humphrey W, Dalke A & Schulten K (1996). VMD: visual molecular dynamics. *J Mol Graph* **14**, 33–38, 27–28.

Jorgensen WL, Chandrasekhar J, Madura JD, Impey RW & Klein ML (1983). Comparison of simple potential functions for simulating liquid water. *J Chem Phys* **79**, 926–935.

Koch MC, Steinmeyer K, Lorenz C, Ricker K, Wolf F, Otto M, Zoll B, Lehmann-Horn F, Grzeschik KH & Jentsch TJ (1992). The skeletal muscle chloride channel in dominant and recessive human myotonia. *Science* **257**, 797–800.

Lakraj AA, Miller G, Vortmeyer AO, Khokhar B, Nowak RJ & DiCapua DB. (2013). Novel mutations in the CLCN1 gene of myotonia congenita: 2 case reports. *Yale J Biol Med* **86**, 101–106.

Lo Monaco M, D'Amico A, Luigetti M, Desaphy JF & Modoni A (2014). Effect of mexiletine on transitory depression of compound motor action potential in recessive myotonia congenita. *Clin Neurophysiol* **126**, 399–403.

Lossin C & George AL Jr (2008). Myotonia Congenita. *Adv Genet* **63**, 25–55.

Ma L, Rychkov GY, Bykova EA, Zheng J & Bretag AH (2011). Movement of hClC-1 C-termini during common gating and limits on their cytoplasmic location. *Biochem J* **436**, 415–28.

Macias MJ, Teijido O, Zifarelli G, Martin P, Ramirez-Espain X, Zorzano A, Palacin M, Pusch M & Estevez R (2007). Myotonia-related mutations in the distal C-terminus of ClC-1 and ClC-0 chloride channels affect the structure of a poly proline helix. *Biochem J* **403**, 79–87.

MacKerell AD Jr, Banavali N & Foloppe N (2000). Development and current status of the CHARMM force field for nucleic acids. *Biopolymers* **56**, 257–265.

Mangiatordi GF, Alberga D, Siragusa L, Goracci L, Lattanzi G & Nicolotti O (2015). Challenging AQP4 druggability for NMO-IgG antibody binding using molecular dynamics and molecular interaction fields. *Biochim Biophys Acta* **1848**, 1462–1471.

Markhorst JM, Stunnenberg BC, Ginjaar IB, Drost G, Erasmus CE & Sie LT (2014). Clinical experience with long-term acetazolamide treatment in children with nondystrophic myotonias: a three-case report. *Pediatr Neurol* **51**, 537–541.

Martyna GJ, Tobias DJ & Klein ML (1994). Constant pressure molecular dynamics algorithms. *J Chem Phys* **101**, 4177–4189.

Matthews E, Fialho D, Tan SV, Venance SL, Cannon SC, Sternberg D, Fontaine B, Amato AA, Barohn RJ, Griggs RC, Hanna MG & the CINCH Investigators (2010). The non-dystrophic myotonias: molecular pathogenesis, diagnosis and treatment. *Brain* **133**, 9–22.

Mazón MJ, Barros F, Dela Peña P, Quesada JF, Escudero A, Cobo AM, Pascual-Pascual SI, Gutiérrez-Rivas E, Guillén E, Arpa J *et al.* (2012). Screening for mutations in Spanish families with myotonia. Functional analysis of novel mutations in CLCN1 gene. *Neuromuscul Disord* **22**, 231–43.

Meyer-Kleine C, Steinmeyer K, Ricker K, Jentsch TJ & Koch MC (1995). Spectrum of mutations in the major human skeletal muscle chloride channel gene (CLCN1) leading to myotonia. *Am J Hum Genet* **57**, 1325–1334.

Miyamoto S & Kollman PA (1992). Settle: An analytical version of the SHAKE and RATTLE algorithm for rigid water models. *J Comput Chem* **13**, 952–962.

Papponen H, Nissinen M, Kaisto T, Myllylä VV, Myllylä R & Metsikkö K (2008). F413C and A531V but not R894X myotonia congenita mutations cause defective endoplasmic reticulum export of the muscle-specific chloride channel CLC-1. *Muscle Nerve* **37**, 317–325.

Phillips JC, Braun R, Wang W, Gumbart J, Tajkhorshid E, Villa E, Chipot C, Skeel RD, Kalé L & Schulten K (2005). Scalable molecular dynamics with NAMD. *J Comput Chem* **26**, 1781–1802.

Pusch M, Accardi A, Liantonio A, Guida P, Traverso S, Camerino DC & Conti F (2002). Mechanisms of block of muscle type CLC chloride channels. *Mol Membr Biol* **19**, 285–92.

Pusch M, Steinmeyer K, Koch MC & Jentsch TJ (1995). Mutations in dominant human myotonia congenita drastically alter the voltage dependence of the CIC-1 chloride channel. *Neuron* **15**, 1455–1463.

Raja Rayan DL & Hanna MG (2010). Skeletal muscle channelopathies: nondystrophic myotonias and periodic paralysis. *Curr Opin Neurol* **23**, 466–76.

Raja Rayan DL, Haworth A, Sud R, Matthews E, Fialho D, Burge J, Portaro S, Schorge S, Tuin K, Lunt P *et al.* (2012). A new explanation for recessive myotonia congenita: exon deletions and duplications in CLCN1. *Neurology* **78**, 1953–1958.

Richardson RC, Tarleton JC, Bird TD & Gospe SM Jr (2014). Truncating CLCN1 mutations in myotonia congenita: variable patterns of inheritance. *Muscle Nerve* **49**, 593–600.

Richman DP, Yu Y, Lee TT, Tseng PY, Yu WP, Maselli RA, Tang CY & Chen TY (2012). Dominantly inherited myotonia congenita resulting from a mutation that increases open probability of the muscle chloride channel CLC-1. *Neuromolecular Med* **14**, 328–337.

Ryckaert J-P, Ciccotti G & Berendsen HJC (1977). Numerical integration of the cartesian equations of motion of a system with constraints: molecular dynamics of *n*-alkanes. *J Comput Phys* **23**, 327–341.

Saviane C, Conti F & Pusch M (1999). The muscle chloride channel ClC-1 has a double-barreled appearance that is differentially affected in dominant and recessive myotonia. *J Gen Physiol* **113**, 457–468.

Schrödinger Release 2013-2: Maestro, version 9.5, Schrödinger, LLC, New York, NY, 2013.

Simpson BJ, Height TA, Rychkov GY, Nowak KJ, Laing NG, Hughes BP & Bretag AH (2004). Characterization of three myotonia-associated mutations of the CLCN1 chloride channel gene via heterologous expression. *Hum Mutat* **24**, 185–191.

Skálová D, Zídková J, Voháňka S, Mazanec R, Mušová Z, Vondráček P, Mrázová L, Kraus J, Réblová K & Fajkusová L (2013). CLCN1 mutations in Czech patients with myotonia congenita, *in silico* analysis of novel and known mutations in the human dimeric skeletal muscle chloride channel. *PLoS One* **8**, e82549.

Stölting G, Fischer M & Fahlke C (2014*a*). CLC channel function and dysfunction in health and disease. *Front Physiol* **5**, 378 doi: 10.3389/fphys.2014.00378.

Stölting G, Fischer M & Fahlke, C (2014*b*). ClC-1 and ClC-2 form hetero-dimeric channels with novel protopore functions. *Pflugers Arch* **466**, 2191–204.

Trivedi JR, Cannon SC & Griggs RC (2014). Nondystrophic myotonia: Challenges and future directions. *Exp Neurol* **253**, 28–30.

Tseng PY, Yu WP, Liu HY, Zhang XD, Zou X & Chen TY (2011). Binding of ATP to the CBS domains in the C-terminal region of CLC-1. *J Gen Physiol* **137**, 357–368.

Ulzi G, Lecchi M, Sansone V, Redaelli E, Corti E, Saccomanno D, Pagliarani S, Corti S, Magri F, Raimondi M *et al.* (2012). Myotonia congenita: Novel mutations in CLCN1 gene and functional characterizations in Italian patients. *J Neurol Sci* **318**, 65–71.

Ulzi G, Sansone VA, Magri F, Corti S, Bresolin N, Comi GP & Lucchiari S (2014). *In vitro* analysis of splice site mutations in the CLCN1 gene using the minigene assay. *Mol Biol Rep* **41**, 2865–2874.

Weinberger S, Wojciechowski D, Sternberg D, Lehmann-Horn F, Jurkat-Rott K, Becher T, Begemann B, Fahlke C & Fischer M (2002). Disease-causing mutations C277R and C277Y modify gating of human ClC-1 chloride channels in myotonia congenita. *J Physiol* **590**, 3449–3464.

Zhang J, George AL Jr, Griggs RC, Fouad GT, Roberts J, Kwieciński H, Connolly AM & Ptácek LJ (1996). Mutations in the human skeletal muscle chloride channel gene (CLCN1) associated with dominant and recessive myotonia congenita. *Neurology* **47**, 993–998.

Additional information

Competing interests

The authors declare no competing interests.

Author contributions

P.I. and D.C.C. conceived and designed the experiments. L.M., R.M., G.L., G.R., G.S., G.A. and R.M. performed

the clinical diagnosis of the four families at Istituto Besta, Milan, at University of Pisa and at Spedali Civili, Brescia and at A.Re.S. Puglia, Bari. P.B. and R.B. performed the molecular genetics diagnosis of MC patients at Istituto Besta, Milan. Mutagenesis was performed by M.M.D. and expression studies were performed by C.A. at University of Bari. Electrophysiological experiments were performed and analysed by P.I. and J.-F.D. at University of Bari. G.M., D.A., G.L. and O.N. performed and analysed the MD simulations at University of Bari. P.I, R.M and D.C.C. drafted the manuscript with input from the co-authors. All authors approved the final version of the manuscript.

Funding

This work was supported by the Italian Department of Health (GR-2009-1580433 to P.I.) and the Italian Telethon Foundation (grants GGP10101 and GGP14096 to D.C.C.).

Acknowledgements

We would like to thank Brett Bennetts and Michael Parker for kindly providing the homology model of hClC-1 based on the crystallographic coordinates of CmClC.